

Horizontal hydrodynamic coupling between shuttle tanker and FPSO arranged side-by-side

Hong-Chao Wang* and Lei Wang

State Key Laboratory of Ocean Engineering, Shanghai Jiao Tong University, Shanghai 200240, China

(Received September 27, 2012, Revised November 11, 2013, Accepted November 20, 2013)

Abstract. Side-by-side offloading operations are widely utilized in engineering practice. The hydrodynamic interactions between two vessels play a crucial role in safe operation. This study focuses on the coupled effects between two floating bodies positioned side-by-side as a shuttle tanker-FPSO (floating production, storage and offloading) system. Several wave directions with different side-by-side distances are studied in order to obtain the variation tendency of the horizontal hydrodynamic coefficients, motion responses and mean drift forces. It is obtained that the coupled hydrodynamics between two vessels is evidently distinguished from the single body case with shielding and exaggerating effects, especially for sway and yaw directions. The resonance frequency and the peak amplitude are closely related with side-by-side separation distance. In addition, the horizontal hydrodynamics of the shuttle tanker is more susceptible to coupled effects in beam waves. It is suggested to expand the gap distance reasonably in order to reduce the coupled drift forces effectively. Attention should also be paid to the second peaks caused by hydrodynamic coupling. Since the horizontal mean drift forces are the most mainly concerned forces to be counteracted in dynamic positioning (DP) system and mooring system, prudent prediction is beneficial in saving consumed power of DP system and reducing tension of mooring lines.

Keywords: hydrodynamic coupling; side-by-side offloading; horizontal motion; wave drift force; middle-field method; dynamic positioning

1. Introduction

Nowadays, offshore offloading operations take place in many locations throughout the world as oil and gas fields move into deep sea. Side-by-side offloading and stern-to-bow (tandem) offloading are the main options for the direct transfer of product from the FPSO to the shuttle tanker. An example of such an offloading system is a floating oil or gas production annex storage facility, to which an export tanker is positioned by mooring system or DP system during loading operations like oil or gas transfer which is much cheaper than installing new underwater pipelines in remote deep water. This study discusses the hydrodynamic coupling in the first order motions of, and the mean second order drift forces on two vessels, i.e., a FPSO and a shuttle tanker floating abreast freely in regular waves. From the results, the motion responses and mean drift forces of the shuttle tanker are susceptible to the hydrodynamic interactions due to the presence of the FPSO. Therefore, it is of crucial importance to take the hydrodynamic interactions into account to assure

*Corresponding author, Associate Professor, E-mail: wanglei@sjtu.edu.cn

safe offloading operations. In addition, shuttle tanker is often equipped with a dynamic positioning system for independent operation in extreme weather conditions. In the DP configuration, the shuttle tanker follows a reference point on the FPSO in order to minimize relative motion between the vessels. As DP system usually takes the horizontal motions into account, getting a better perspective of the horizontal motions and drift forces is beneficial for both the control of a shuttle tanker with DP system and prediction of the behavior for safe operation. The analysis is helpful to both prudent designs in basic design stage and operations in engineering practice.

As for the hydrodynamic interactions between multiple bodies, Ohkusu (1976) analyzed the motions of a ship in the neighborhood of a large moored 2D floating structure by strip theory. Kodan (1984) extended Ohkusu's theory to hydrodynamic interaction problem between two parallel structures in oblique waves. Choi and Hong (2002) employed an HOBEM (higher order boundary element method) to study 3D hydrodynamic interactions between two vessels. Huijsmans *et al.* (2001) found that numerical exaggeration occurred due to numerical inaccuracy in constant panel method when the distance between two vessels is very close and a lid technique was presented to circumvent unrealistic high water velocities on the ship's hull. Masashi (2005) utilized near-field formulation with HOBEM to investigate wave drift forces and moments on two ships arranged side by side in waves. Lee *et al.* (2007) studied the effects of LNG-tank sloshing and found that the most pronounced coupled effects are the shift or split of peak-motion frequencies. Kristiansen and Faltinsen (2010) studied the coupled resonant response of a ship and a fixed terminal. Lu *et al.* (2011) investigated the dependence of the wave forces of multiple bodies in close proximity on the incident wave frequency based on both the viscous fluid and the potential flow models. Zhao *et al.* considered hydrodynamic and mechanical coupling effects utilizing SIMO and focused on their effects on the connection system between two vessels. Kang and Kim (2012) studied the effects of non-collinear wind-wave-current environmental forces on hydrodynamic interactions and coupled dynamics between multiple bodies.

2. Theoretical background

2.1 Boundary conditions

On the basis of the perturbation method, the linearized boundary value problem must be settled first, and then the drift forces and moments can be computed only from quadratic products of the first-order quantities. According to linear potential theory, the potential of a floating body is a superposition of the potentials due to the undisturbed incoming wave Φ_I , the potential due to the diffraction of the undisturbed incoming wave on the fixed body Φ_D and the radiation potentials due to the six body motions Φ_R

$$\Phi(x, y, z; t) = \Phi_I + \Phi_D + \Phi_R \quad (1)$$

Since frequency problem is dedicated to seeking the stationary solution, the total potential Φ can be split as a product of a space-dependent term and a harmonic time-dependent term

$$\Phi(x, y, z; t) = \text{Re} \left[\phi(x, y, z; t) \cdot e^{-i\omega t} \right] \quad (2)$$

Here Re in Eq. (2) means the real part to be taken. Note that the real part symbol Re is neglected for convenience in the remainder of this section and only the boundary conditions of the

space-dependent part are listed. The incident wave potential for deep water is

$$\Phi_I = \text{Re}(\phi_I \cdot e^{-i\omega t}) \quad (3)$$

Then the space-dependent part of the velocity potential associated with an undisturbed long-crest regular wave is given by

$$\phi_I = \zeta_0 g / i\omega \cdot e^{kz + ik(x \cos \beta + y \sin \beta)} \quad (4)$$

Where ω is the wave frequency, ζ_0 is the amplitude of incident wave, k is the wave number at infinite water depth which is determined by dispersion equation ($k = \omega^2 / g$), β is the relative angle of incidence of a plane progressive wave.

For two vessels in close proximity, because of the shielding effect and the reflection of wave, the hydrodynamic forces on each floating body are different from those of the single body case. Owing to the oscillatory motions of the adjacent floating body, each vessel suffers additional diffraction and radiation forces. The resultant velocity potentials on ship A and B can be written as

$$\begin{cases} \phi_a = \phi_I + \phi_{Daa} + \phi_{Dba} + \sum_{j=1}^6 \phi_{Rjaa} + \sum_{j=1}^6 \phi_{Rjba} \\ \phi_b = \phi_I + \phi_{Dbb} + \phi_{Dab} + \sum_{j=1}^6 \phi_{Rjbb} + \sum_{j=1}^6 \phi_{Rjab} \end{cases} \quad (5)$$

Where ϕ_I is the incident wave potential; ϕ_{Daa}, ϕ_{Dba} are the diffraction potentials of ship A due to the presence of ship A and ship B, respectively; ϕ_{Rjaa}, ϕ_{Rjab} are the j th mode radiation potentials of ship A and ship B due to the oscillation of ship A while ship B is restrained, $j=1, 2, \dots, 6$ for surge, sway, heave, roll, pitch and yaw, respectively. The similar situation goes with ϕ_{Dbb}, ϕ_{Dab} and ϕ_{Rjbb}, ϕ_{Rjba} .

The flows are treated here being non-viscous, incompressible, continuous and homogeneous. There are no cavitation holes or gas bubbles in the fluid. Thus, the fluid satisfies the Laplace equation

$$\nabla^2 \phi = 0 \quad \text{for } z \leq 0 \quad (6)$$

The boundary conditions on free surface and sea bottom are

$$-\omega^2 \phi + g \cdot \frac{\partial \phi}{\partial z} = 0 \quad \text{at } z = 0 \quad (7)$$

$$\partial \phi / \partial z = 0 \quad z \rightarrow -\infty \quad (8)$$

All potentials satisfy the above conditions whereas have differences on the body conditions. When considering diffraction problem, it is assumed that the waves are approaching a restrained body. Then the body boundary conditions for diffraction potentials become

$$\begin{cases} \frac{\partial}{\partial n} (\phi_I + \phi_{Daa} + \phi_{Dba}) = 0 & \text{on } S_A \\ \frac{\partial}{\partial n} (\phi_I + \phi_{Dbb} + \phi_{Dab}) = 0 & \text{on } S_B \end{cases} \quad (9)$$

When ship A is oscillating while ship B is fixed, the body boundary conditions for radiation potentials are shown in Eq. (10). On the contrary, when ship B is oscillating while ship A is restrained, the body boundary conditions have similar expression as shown in Eq. (11).

$$\begin{cases} \frac{\partial}{\partial n} \phi_{Rjaa} = -i\omega n_j \quad (j=1,2,\dots,6) & \text{on } S_A \\ \frac{\partial}{\partial n} \phi_{Rjab} = 0 & \text{on } S_B \end{cases} \quad (10)$$

$$\begin{cases} \frac{\partial}{\partial n} \phi_{Rjba} = 0 & \text{on } S_A \\ \frac{\partial}{\partial n} \phi_{Rjbb} = -i\omega n_j \quad (j=1,2,\dots,6) & \text{on } S_B \end{cases} \quad (11)$$

2.2 Numerical procedure

For potential flows, the integrals over the fluid domain can be transformed to integrals over the boundaries of the fluid domain. This allows the application of panel or boundary element methods to solve the 3D potential theory problem. Panel methods divide the surface of the ship and the surrounding water into discrete elements. On each of these elements a distribution of sources is defined that fulfill the Laplace equation. Applying the three-dimensional source distribution method, then the diffraction and radiation potential can be represented by the distribution with the source strength $\sigma(Q)$ on the surface S_A and S_B in the form

$$\iint_{S_A+S_B} \sigma(Q)G(P,Q)ds(Q) = 4\pi\varphi(P) \quad \text{for } P \text{ inside fluid} \quad (12)$$

Where the Green's Function $G(P,Q)$ is a source function at the field point P due to an unknown source density at the source point Q which satisfies $\nabla^2 G(P,Q) = 4\pi\delta(P-Q)$. Extensive studies on $G(P,Q)$ can be found in Noblesse (1982) and Newman (1992). The unknown source strength $\sigma(Q)$ can be obtained by imposing the body boundary condition Eqs. (9)-(11), then the corresponding boundary conditions for diffraction and radiation potentials on S_A and S_B can be expressed as

$$-\frac{1}{2}\sigma(P) + \frac{1}{4\pi} \iint_{S_A+S_B} \sigma(Q) \frac{\partial G(P,Q)}{\partial n} ds(Q) = V_n \quad (13)$$

Where V_n is the normal component of the velocity on the body surface which has been given in Eqs. (9)-(11). By discretizing the mean wetted surface of S_A and S_B into n panels of area S_j , on which the source strength are homogeneously distributed, the following discretized form of equation is obtained

$$-\frac{1}{2}\sigma_j + \frac{1}{4\pi} \sum_{j=1, j \neq i}^N \sigma_j \frac{\partial G(P_i, Q_j)}{\partial n} S_j = V_{ni} \quad (i=1,2,\dots,N) \quad (14)$$

A numerical problem associated with the solution of Eq. (14) is the occurrence of so-called irregular frequencies at which the results are unrealistic. The cause of this problem is the utilization of wave green function method by which the exterior and interior problems are connected. Meanwhile, the integrals over the exterior and interior free surfaces disappear by adopting Dirichlet type condition. However, it is well-known that at some frequencies, this kind of boundary value problem possesses nontrivial solutions. The numerical consequence of this is the matrix of the linear system of equations becomes ill-conditioned and the results are erroneous around these frequencies. It is noteworthy that irregular frequencies are associated with eigen frequencies of the internal non-physical flow of the body and increasing the number of panels does not remove the irregular frequencies. Malenica and Chen (1998) proposed an effective method to reduce the effects of irregular frequencies, which is, among others, to “close” the body by means of discretization of the free surface inside the body (putting a “lid” on the free surface inside the body). The lowest irregular frequency for a parallelepiped is

$$\omega_{irr} = \sqrt{kg} / \tanh kT \quad \text{with} \quad k = \pi \sqrt{B^{-2} + L^{-2}} \quad (15)$$

Where (L, B, T) are the length, width and draft of the box. For a ship, the lowest irregular frequency is close to that estimated by above Eq. (15) using ship’s length, width and draft of the box. The position of the inside free surface z_{max} should satisfy Eq. (16) to ensure that there will not be any irregular frequencies within the frequency area from 0 to ω_{max} which is the maximum wave frequency we are interested in.

$$z_{max} \leq \tanh^{-1} \left(\frac{kg}{\omega_{max}^2} \right) / k \quad (16)$$

The irregular frequencies are eliminated in this paper by generating a mesh on the vessel’s water-plane and modifying the original integral equation by extending the singularity support to the internal water-plane.

2.3 Wave induced forces and hydrodynamic coefficients

The forces and moments follow an integration of the pressure over the submerged body surface B , i.e., S_A or S_B

$$\begin{cases} F_a^{(1)} = \iint_{S_A} (p^{(1)} \cdot n) \cdot ds = -\rho \iint_{S_A} \left(\frac{\partial \phi_I}{\partial t} + \sum_{j=1}^6 \frac{\partial \phi_{Rjaa}}{\partial t} + \sum_{j=1}^6 \frac{\partial \phi_{Rjba}}{\partial t} + \frac{\partial \phi_{Daa}}{\partial t} + \frac{\partial \phi_{Dba}}{\partial t} + gz \right) n \cdot ds \\ F_b^{(1)} = \iint_{S_B} (p^{(1)} \cdot n) \cdot ds = -\rho \iint_{S_B} \left(\frac{\partial \phi_I}{\partial t} + \sum_{j=1}^6 \frac{\partial \phi_{Rjbb}}{\partial t} + \sum_{j=1}^6 \frac{\partial \phi_{Rjab}}{\partial t} + \frac{\partial \phi_{Dbb}}{\partial t} + \frac{\partial \phi_{Dab}}{\partial t} + gz \right) n \cdot ds \end{cases} \quad (17)$$

In which $F_a^{(1)}$ and $F_b^{(1)}$ are the wave induced forces exerted on ship A and ship B , respectively; n is the outward normal vector on the body surface B .

The hydrodynamic added mass and damping coefficients of the radiation forces are given by

$$\begin{cases}
A_{jkaa} = -\text{Re} \left\{ \rho \iint_{S_A} \phi_{Rjaa} n_k \cdot ds \right\} & \text{and } B_{jkaa} = -\text{Im} \left\{ \rho \omega \iint_{S_A} \phi_{Rjaa} n_k \cdot ds \right\} \\
A_{jkba} = -\text{Re} \left\{ \rho \iint_{S_A} \phi_{Rjba} n_k \cdot ds \right\} & \text{and } B_{jkba} = -\text{Im} \left\{ \rho \omega \iint_{S_A} \phi_{Rjba} n_k \cdot ds \right\} \\
A_{jbb a} = -\text{Re} \left\{ \rho \iint_{S_B} \phi_{Rjbb} n_k \cdot ds \right\} & \text{and } B_{jbb a} = -\text{Im} \left\{ \rho \omega \iint_{S_B} \phi_{Rjbb} n_k \cdot ds \right\} \\
A_{jkab} = -\text{Re} \left\{ \rho \iint_{S_B} \phi_{Rjba} n_k \cdot ds \right\} & \text{and } B_{jkab} = -\text{Im} \left\{ \rho \omega \iint_{S_B} \phi_{Rjba} n_k \cdot ds \right\}
\end{cases} \quad (18)$$

Where A and B represent the added mass and damping coefficients, take A_{jkba} as an illustration, it stands for the added mass of ship A due to the motion of ship B in case of an oscillation of ship B in the direction j with a velocity potential of ϕ_{Rjba} and so do the other coefficients.

2.4 Equations of motions

After solving the above exciting forces, added mass and damping coefficients, the motions of two ships can be solved by a set of 12 coupled equations of motions shown as below

$$\begin{cases}
\sum_{j=1}^6 \left\{ [-\omega^2 (M_a + A_{jkaa}) - i\omega B_{jkaa} + C_a] \zeta_{ja} + [-\omega^2 A_{jkba} - i\omega B_{jkba}] \zeta_{jb} \right\} = \tau_a \\
\sum_{j=1}^6 \left\{ [-\omega^2 (M_b + A_{jbb a}) - i\omega B_{jbb a} + C_b] \zeta_{jb} + [-\omega^2 A_{jkab} - i\omega B_{jkab}] \zeta_{ja} \right\} = \tau_b
\end{cases} \quad (19)$$

In which $\tau_a = -\rho \iint_{S_A} \left(\frac{\partial \varphi_I}{\partial t} + \frac{\partial \varphi_{Daa}}{\partial t} + \frac{\partial \varphi_{Dba}}{\partial t} \right) n \cdot ds$ and $\tau_b = -\rho \iint_{S_B} \left(\frac{\partial \varphi_I}{\partial t} + \frac{\partial \varphi_{Dbb}}{\partial t} + \frac{\partial \varphi_{Dab}}{\partial t} \right) n \cdot ds$; M and C are the mass of ship and restoring force with the suffix a and b which stand for ship A and ship B , respectively. ζ_{ja} and ζ_{jb} are the j th mode of ship A and ship B , respectively, $j=1,2,\dots,6$ for surge, sway, heave, roll, pitch and yaw, respectively.

By solving the motion equations in the frequency domain, the RAO (Response Amplitude Operator) for the vessels' motions can be derived. These parameters are conventionally employed to manifest the hydrodynamic behaviors of the vessels.

2.5 Middle-field formulation of wave mean drift loads

The solution of the second-order problem results in mean drift forces and forces oscillating with difference frequency and sum frequency in addition to the linear solution. For mean drift loads, two classical formulations have been developed. One of these consists of direct pressure integrations on the hull of the body which is called near-field formulation. Another is derived by applying the momentum theorem to the fluid domain and is called the far-field formulation. The near-field formulation is general as it can be used to obtain all components of wave mean drift loads applied to a single body or multiple bodies while the far-field formulation is restricted to give only three horizontal components, i.e., global mean surge and sway forces and the mean yaw moments. However, the numerical robustness of near-field method is not as good as far-field

method.

Chen (2007) developed a new method called middle-field formulation involving control surfaces at some distance from the body which is as robust as the far-field formulation and as general as the near-field formulation of mean drift loads on a single body as well as on multiple bodies. By applying Gauss’s theorem to the domain limited by the control surface, a formulation is given which involves integrals on the control surface and along its intersection with the mean free surface, and the part of free surface limited by the intersection and the waterline. Middle-field method provides a formal connection between the near-field and far-field formulations and it can be applied to multiple bodies to gain all components of mean drift loads with good convergence and numerical stability. For mean drift forces, computation can be considered without the contribution of the second-order time-harmonic potential. In addition, the static second-order forces due to the first order motions which give only non-zero values for the vertical force and moments around the horizontal axes can be evaluated without any numerical difficulty. Detailed deduction can be found in Chen (2007).

3. Numerical side-by-side system model

In order to describe the motion responses between two floating structures, three sets of right-handed orthogonal coordinate frames are utilized as shown in Fig. 1(a). The first system of coordinate axes $\{n\} = (X, Y, Z)$ is a right-handed earth-bound axes system with origin O , X – and Y – axes in the mean free surface of the sea and Z – axis positive upwards. The two body-fixed reference frames $\{b_a\} = (x_a, y_a, z_a)$ with origin O_a and $\{b_b\} = (x_b, y_b, z_b)$ with origin O_b are moving coordinate frames that are fixed to ship A and ship B , respectively. For each of the body-fixed frames, z – axis is oriented upward, x – axis points to ship’s bow and y – axis to the portside. The direction of incident wave is defined as shown in Fig. 1(b).

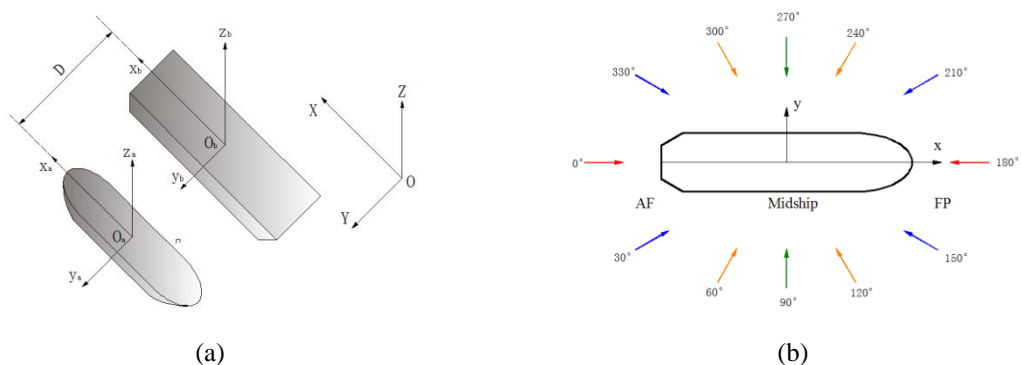
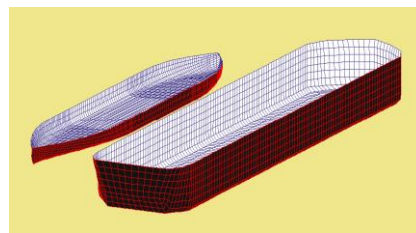


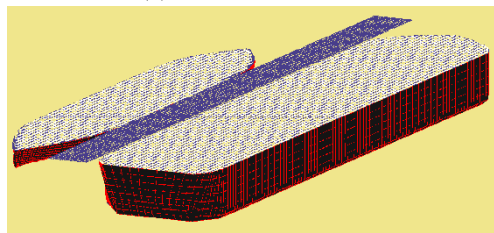
Fig. 1 Definition of coordinate frames and direction of incident wave

The principal dimensions of the shuttle tanker and the FPSO are listed in Table 1. The wetted surfaces of the shuttle tanker and the FPSO are discretized into 2880 and 2704 elements,

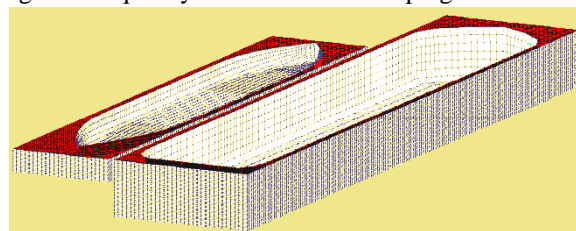
respectively. Fig. 2(a) shows the mesh model of the shuttle tanker-FPSO system situated side-by-side. Within the framework of the potential theory there is no limit in predicting resonant wave elevation while in reality the resonant motion is largely damped by different mechanisms of dissipation. In this paper, the problem is solved by establishing the mesh at the gap as the damping zone which is illustrated in Fig. 2(b). In addition, it is common to include a linearized viscous damping to account for the strong non-linearity of the damping force. For simplicity the viscous damping is often taken as a fraction of the critical damping. In this paper, the viscous damping is added as 5 percentage of the critical damping. The mesh for irregular frequency removal inside the vessel is also shown in Fig. 2 (b).



(a) Mesh on the hull



(b) Mesh for irregular frequency removal and damping zone between two vessels



(c) Mesh on the control surface

Fig. 2 Mesh model of shuttle tanker-FPSO system situated side-by-side

When the FPSO and the shuttle tanker are situated side-by-side with relatively small gap, the computation results of the motion responses of the two vessels behave almost the same. However, compared with the FPSO, the shuttle tanker is more susceptible to the hydrodynamic interactions incurred by the presence of the FPSO from the calculation results. Therefore, in this paper, only the hydrodynamic results of the shuttle tanker are shown. Due to the fact that the separation distances between the two vessels are usually less than 30m during the operation of equipment or supplies transfer from one vessel to the other, the spacing distances are selected as 4 m, 6 m, 9 m, 12 m, 15 m, 20 m. The frequency area is chosen from 0.0 to 1.5 with a calculation step of

0.05rad/s. For some frequency areas where peaks are steep, the time step is chosen to be 0.01 rad/s. This paper computes the hydrodynamics of the shuttle tanker in several wave directions, i.e., head wave ($\beta = 180^\circ$), stern wave ($\beta = 0^\circ$), leeside waves ($\beta = 30^\circ, 60^\circ, 90^\circ$) and weather side waves ($\beta = 210^\circ, 240^\circ, 270^\circ$).

Table 1 Principal dimensions of FPSO and shuttle tanker

Designation	Symbol	Unit	FPSO	Shuttle tanker
Length between perpendiculars	L_{pp}	m	300.4	233.4
Breadth	B	m	58	39.6
Depth	D	m	29.4	19.2
Draft	T	m	20.4	8
Displacement	Δ	ton	349430	86591
Longitudinal center of gravity	LCG	m	2.82	6.25
Center of gravity above keel	VCG	m	16.61	10.74
Metacentric height transverse	GM_t	m	21.62	6.94
Roll radius of gyration	k_{xx}	m	19.33	13.20
Pitch radius of gyration	k_{yy}	m	75.25	58.34

4. Results and discussion

4.1 Added mass and damping coefficients

The hydrodynamic coefficients of the shuttle tanker with different separation distances and the single body case are shown in Fig. 3. Non-dimension is made using $\rho \cdot \nabla$ and $\rho \cdot \nabla \sqrt{g/L}$ for surge and sway added mass and damping coefficients, $\rho \cdot \nabla \cdot BD$ and $\rho \cdot \nabla \cdot BD \sqrt{g/L}$ for yaw added mass and damping coefficients, and kL for frequency, where ∇ is the displacement of the shuttle tanker, L, B, D are the characteristic length, breadth and depth, respectively. When the vessel is zero forward speed, the added mass coefficients stay the same, irrespective of different wave directions and the same situation goes with the damping coefficients. In addition, it is noted that the coefficients are exerted only by wave interactions between the FPSO and the shuttle tanker. From the figure, the hydrodynamic coefficients of single body case stabilize at a comparably low level without any obvious peaks which differs greatly from the multi-body cases, especially for sway and yaw directions. For instance, in sway direction with a gap distance of 4 m, it is observed that the added mass coefficient plunges sharply to negative after a spike, while, for the damping coefficient, the curve soars to the highest point at a non-dimensional kL of 17.2, i.e., 0.85 rad/s, which means that the shuttle tanker becomes more sensitive to external disturbances near the frequency. The other cases experience the trends in the same fashion. With two vessels getting closer, the peak values become larger and the corresponding peak frequencies tend to be higher. The peak frequencies of the added mass and damping coefficients are listed in Table 2.

Table 2 Peak frequencies of hydrodynamic coefficients with different spacing distances

	4 m	6 m	9 m	12 m	15 m	20 m
Peak Frequency of surge added mass (rad/s)	0.85	0.80	0.75	0.70	0.70	0.65
Peak Frequency of surge damping(rad/s)	0.80	0.75	0.70	0.65	0.65	0.60
Peak Frequency of sway added mass (rad/s)	0.85	0.75	0.70	0.65	0.60	0.55
Peak Frequency of sway damping(rad/s)	0.85	0.80	0.70	0.65	0.65	0.60
Peak Frequency of yaw added mass (rad/s)	0.80	0.75	0.70	0.65	0.65	0.60
Peak Frequency of yaw damping(rad/s)	0.85	0.80	0.75	0.70	0.70	0.65

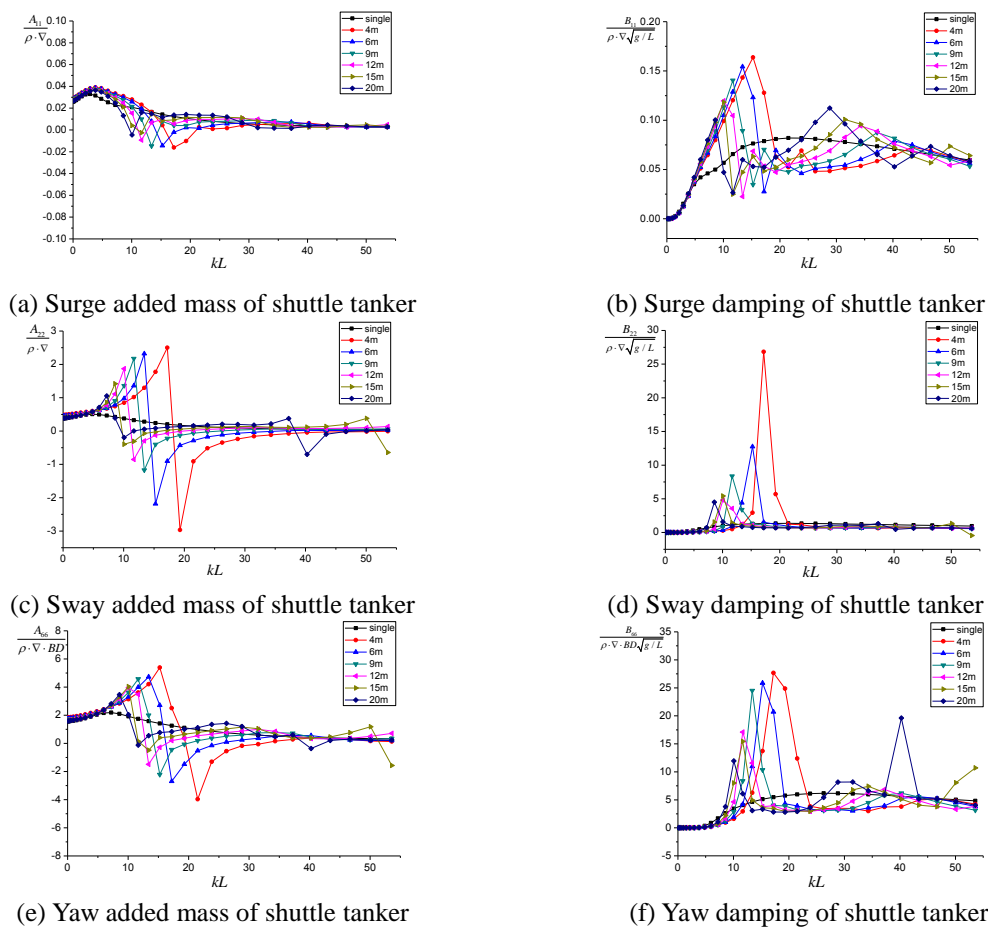


Fig. 3 Hydrodynamic coefficients of shuttle tanker

4.2 First order motion RAO

In this section, the results of hydrodynamic computation are displayed in form of RAO as a vessel's motion response on the wave of unit amplitude. The motion RAOs are depicted in Figs. 4-6 and the hydrodynamic interactions of all cases are properly accounted for. From Fig. 4, it is

seen that surge motions of the single body cases have very small values in beam waves ($\beta = 90^\circ, 270^\circ$) while the largest values are found to be in head and stern waves. Surge motions in all the cases are below 0.1 after 0.6 rad/s and remain the level as the frequency increases. Regarding the coupled cases, the surge motions do not show much difference compared with those of the single body cases within the focused frequency area. Only the beam wave cases exhibit some coupled effects, however, the amplitudes are quite small. As for the discussion in the following part, it is known that coupled effects have more powerful influence on sway and yaw motions under the condition that two vessels are arranged side-by-side due to the sophisticated motions of fluid particles between two vessels. In tandem offshore loading system, however, surge coupled effects are expected to prevail those of the sway motions.

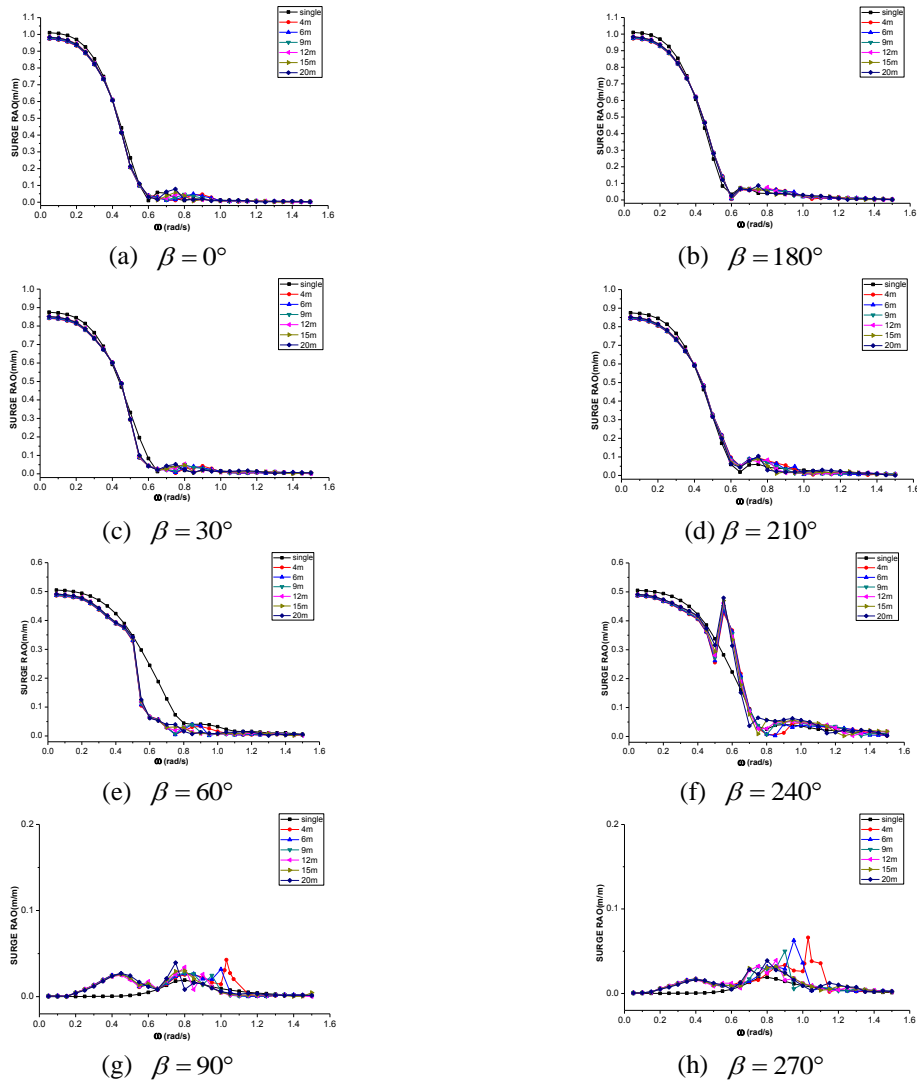


Fig. 4 Surge RAOs of shuttle tanker with different incident wave directions and spacing distances

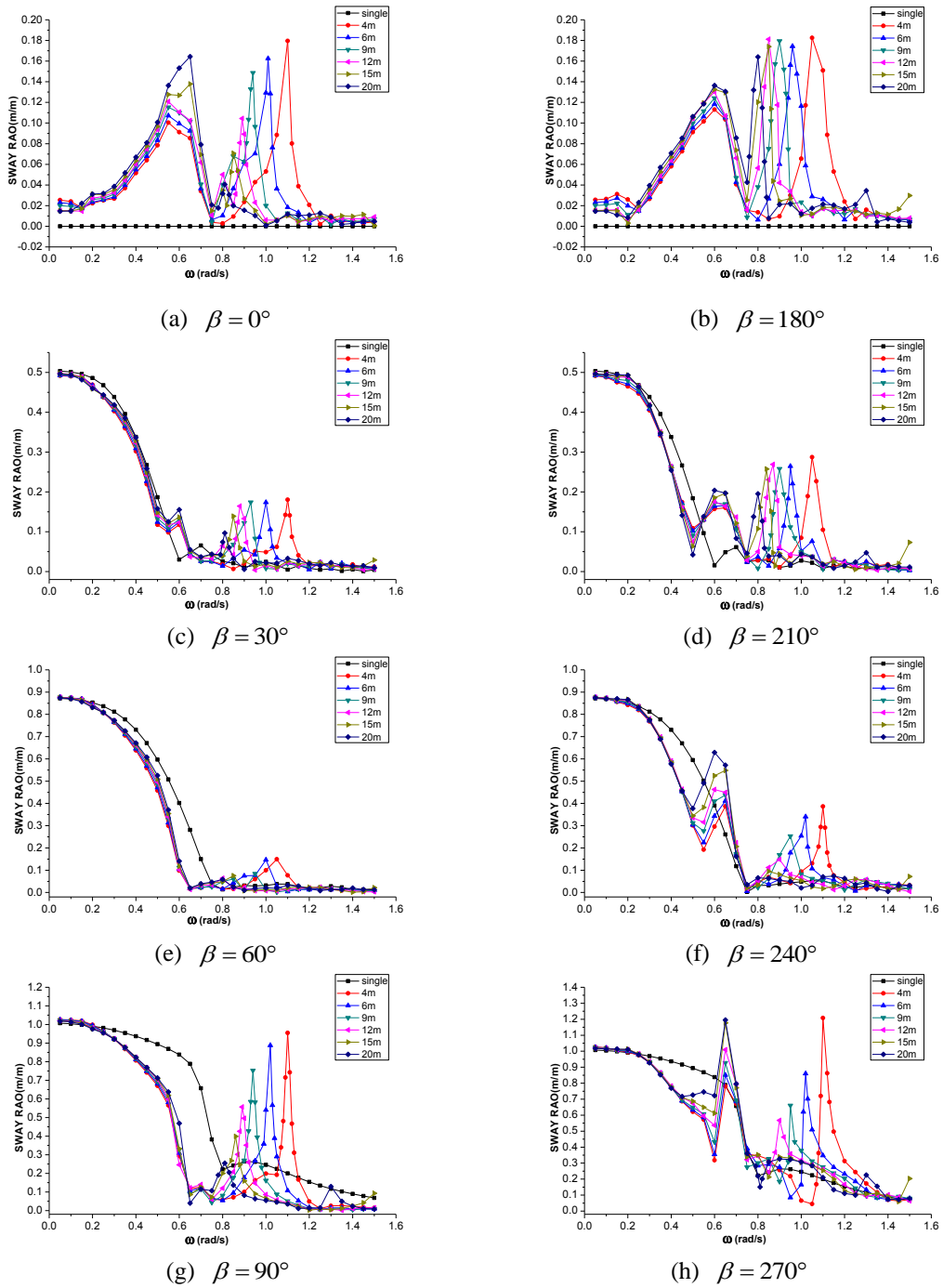


Fig. 5 Sway RAOs of shuttle tanker with different incident wave directions and spacing distances

From Fig. 5, it is seen that when the shuttle tanker floats alone, the sway motion is almost zero in head and stern waves because of the symmetry situation with XOZ plane and it is reasonable that the sway motions in beam waves are the same. There are some nuances between the single body cases in oblique waves since that the bow and the stern of the tanker are not absolutely symmetrical. It can be found that the sway response attains its maximum in beam waves and minimum in head waves among all the wave directions.

When taking the presence of the FPSO into account, the RAO curves exhibit great discrepancies compared with the single body cases in Figs. 5 (a)-5(h). In the low frequency regions, the coupled RAOs behave almost the same with that of the single body case and disparities emerge with the increasing wave frequency. For (a), (b), (d), (f), (h), it is noticed that the coupled RAOs show two obvious peaks. However, in (c), (e), (g), the coupled RAO experiences only one apparent peak. Considering for the two peaks case, declination in gap distances witness slight decreases in the first peak values and obvious increases in the second peak values. These sharp peak responses must relate to resonant phenomena. It can be seen that the difference of gap distances has more overt influence on the magnitude and frequency shift of the second peaks than the first ones, which, illustrates that coupling effects become more important in that range where wave length is short with less diffraction effects. More specifically, the resonance frequencies of the second peaks become higher with the two vessels getting closer. When it comes to the leeside cases with (c), (e), (g), the only peaks have similar variation tendencies according to different gap distances with the second peaks discussed above. Furthermore, the attenuation of the first peaks due to shielding effect can be observed in leeside cases. From (d), (f), (h), it is clearly shown that the sway motion responses become larger when the wave direction is closer to beam wave situation. The results should hold in the same way with (c), (e), (g). However, in contrast to sway motions with 60° incident waves and 90° incident waves, the shielding effect has less influence on the counterparts with 30° incident wave. For this reason, the sway motions with 30° incident waves are a bit larger than that of the 60° incident waves case and small spikes can be observed in (c) at the frequency of 0.6 rad/s which are undermined because of the shielding effect.

When the FPSO and the shuttle tanker are positioned in close proximity of one another in beam waves, the hydrodynamic interactions between the two vessels becomes violent, thus resulting in an appreciable augment of motion responses in comparison with that of the single body case. The harshest response for sway motion can reach 6 times as the counterpart of the single body case, peaking at 1.2 m at 1.10 rad/s in (h) where the phenomenon is a result of the reflection of the waves on the FPSO and radiated waves from the FPSO.

Unlike surge and sway motions, yaw motions have larger values in oblique waves for single body case, which can be observed from Fig. 6. Yaw motions of single body cases are zero for head and stern waves because the shuttle tanker is symmetrical with XOZ plane. In beam waves, yaw motions are almost zero because the bow and the stern are not exactly symmetrical. However, as regards the coupled cases, the beam wave cases experience drastic growth which is the largest even compared with oblique cases. This phenomenon suggests that beam waves tend to have stronger coupled effects on yaw motions. Beam waves can cause the most severe fluid motion between two vessels arranged side-by-side, thus resulting in drastic wave reflection and radiation. Actually, as discussed above, the results turn out to prove that beam waves are the most dangerous direction for side-by-side operations. On the contrary, head and stern waves are much more benign regarding the coupled effects. Concerning the variation trend of yaw motions, it has a lot in common with sway direction. With the gap becoming smaller, yaw motions become larger while peak frequencies tend to be higher.

The results above illustrate that the consideration of hydrodynamic coupling is indispensable for the determination of safe multi-body operations. Mirela Zalar (2007) also calculated the RAOs of coupled motions with different wave directions. Similar tendencies and regularities can be found when compared with the above results.

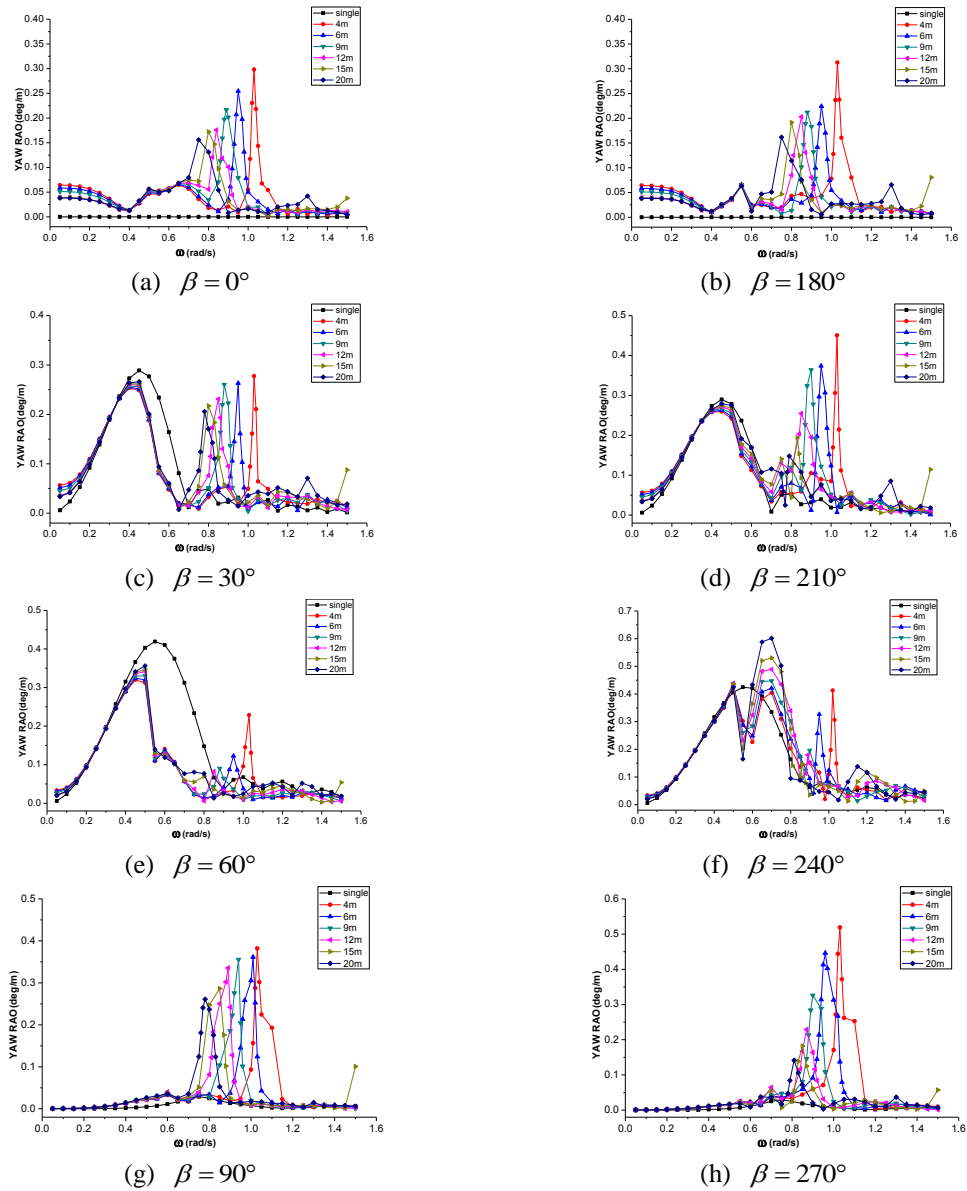


Fig. 6 Yaw RAOs of shuttle tanker with different incident wave directions and spacing distances

Table 3 Peak frequencies of Sway RAOs with different spacing distances

	0°	30°	60°	90°	180°	210°	240°	270°
Sway 4 m	1.10	1.10	1.05	1.10	1.05	1.05	1.10	1.10
Sway 6 m	1.01	1.00	1.00	1.02	0.96	0.95	1.02	1.02
Sway 9 m	0.94	0.93	0.95	0.94	0.90	0.90	0.95	0.95
Sway 12 m	0.89	0.88	0.80	0.89	0.85	0.87	0.90	0.90
Sway 15 m	0.85	0.85	0.85	0.86	0.85	0.84	0.85	0.90
Sway 20 m	0.81	0.81	0.80	0.81	0.80	0.80	0.80	0.90
Yaw 4 m	1.03	1.03	1.03	1.03	1.03	1.03	1.02	1.03
Yaw 6 m	0.95	0.95	0.95	1.01	0.95	0.95	0.95	0.96
Yaw 9 m	0.89	0.88	0.88	0.94	0.88	0.90	0.90	0.90
Yaw 12 m	0.84	0.85	0.85	0.89	0.85	0.85	0.89	0.87
Yaw 15 m	0.80	0.80	0.80	0.85	0.80	0.83	0.86	0.85
Yaw 20 m	0.78	0.78	0.78	0.78	0.78	0.79	0.80	0.81

The peak frequencies of sway and yaw RAOs are shown in Table 3. As can be seen, the resonance frequencies are about 0.20 rad/s to 0.25 rad/s lagging behind that of the hydrodynamic coefficients. From the trend of the hydrodynamic coefficients and RAOs among different side-by-side distances displayed in Figs. 3-6, it is seen that the peak frequencies all diminish with separation distance increasing. For relatively high frequency area where the wavelength is short, the resonance peak may occur due to the standing wave between the shuttle tanker and the FPSO, thus the distance between the two floaters plays a crucial role to determine the resonance peak location. When compare Figs. 3-6, the RAOs do not show much difference in the frequency area where the hydrodynamic coefficients change tremendously, and vice versa. The results highlight the fact that the hydrodynamic interactions between multiple bodies are complex. It is the coupled effect of the added mass and damping coefficients along with other factors to determine the amplitude of the motion responses.

4.3 Mean drift forces

The prediction for mean drift forces is of importance in several contexts for marine structures. As for DP system, the oscillatory first-order wave forces are not considered for thrust resistance in the control closed-loop due to the response time of the thrusters that the DP system cannot compensate the high frequency motions. Moreover, the propulsion system would suffer from high wear and tear and the fuel consumption would increase. Compared with the first-order forces, the second-order mean drift forces must be counteracted by the thrusters to maintain the desired position, otherwise, the marine structures would drift away which may result in marine accidents.

By middle-field method, the horizontal components of mean drift loads involve only a surface integral on the control surface and a line integral along its intersection with the free surface by establishing a control surface surrounding the body. The mesh on the control surface is shown in Fig. 2 (c). Convergence tests have been performed to assure that the mesh we adopt is satisfactory. The horizontal mean drift forces exerted on the shuttle tanker with different separation distances have been calculated with both middle-field and near-field methods. The results show good agreement. Here only the results of middle-field method are displayed in Figs. 7-9. Also wave drift computations are performed for the single body case for the comparison of hydrodynamic

coupling. Non-dimension is made using $\rho g \zeta_a^2 L$ for surge and sway mean drift forces, $\rho g \zeta_a^3 L$ for yaw mean drift forces and $\omega \cdot \sqrt{V^{1/3}} / g$ for frequency, where ζ_a is the wave amplitude.

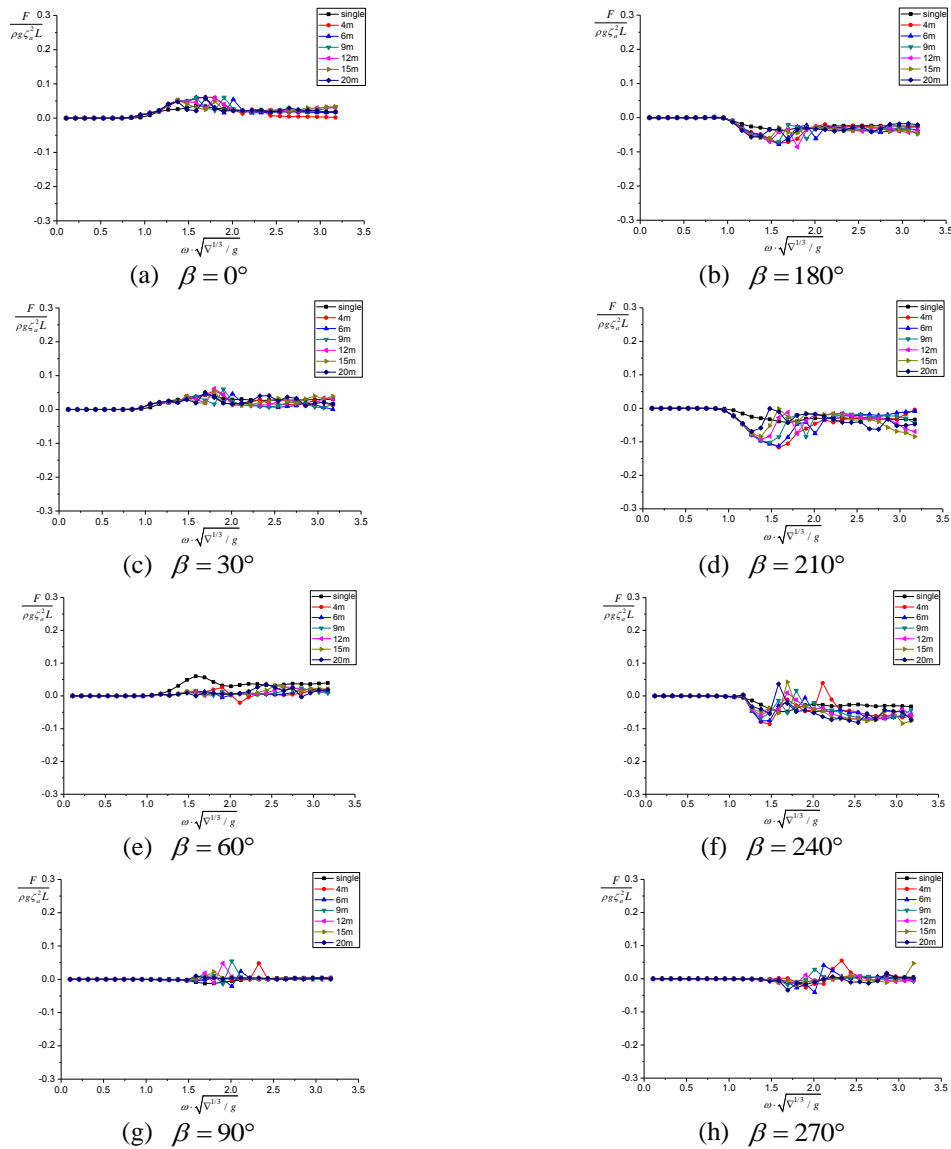


Fig. 7 Surge mean drift forces of shuttle tanker with different wave directions and spacing distances

From Fig. 7, the trend levels off in the studied frequency area. For both the single body cases and the coupled cases, surge drift forces are quite small. Some of the coupled cases experience slight change with small amplitudes. It boils down to the conclusion that coupled effects play less important role in surge direction in side-by-side operations.

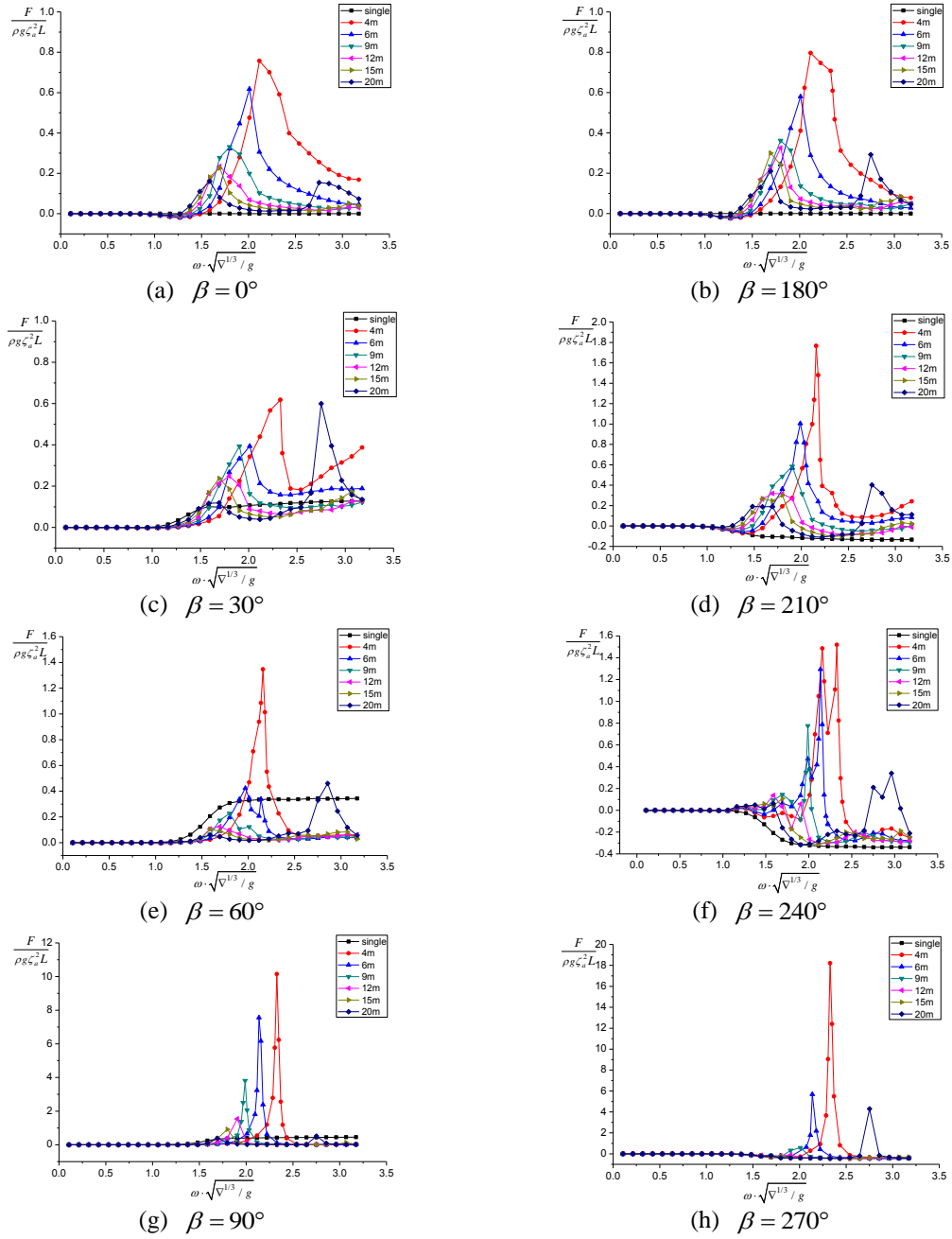


Fig. 8 Sway mean drift forces of shuttle tanker with different wave directions and spacing distances

For sway drift forces in Fig. 8, when the shuttle tanker floats alone, the mean drift forces are nearly zero in head and stern waves while the mean drift forces become positive in leeward oblique waves and negative in weather side oblique waves with the increasing non-dimensional frequency. It is due to the fact that the mean drift force acting on a floating body is in the downwave direction in most cases, thus floating bodies, like the wave particles themselves, drift slowly in the same direction as the incident waves. The variation tendencies of peaks observed in Fig. 8 are similar with that of the second peaks discussed above in Figs. 4-6. Here the resonance frequencies are almost the same with those of the RAOs. Besides, shielding effect can also be observed in the figure. In the relatively high frequency area, the drift force curves of the multi-body cases experience large sharp spikes at resonance frequencies. What's more, the values of mean drift forces become positive in weather side oblique waves. This phenomenon is very similar with the experiment conducted by Ohkusu (1976). He demonstrated a remarkable discovery when he analyzed a small ship lying in beam seas near the weather side of a large fixed vessel. The physical explanation for this phenomenon is due to the fact that resonant standing waves occur at critical values of the separation distance between the two vessels, and the resulting radiation stress effectively pushes the two vessels apart. It is noteworthy that the case for a gap distance of 20 m has another peak in the high frequency area. Actually, with the interested frequency area becoming larger, the cases of other gap distances will also exhibit similar peaks and tendencies as described above. More peaks will occur only if resonant conditions with certain system configuration are fulfilled.

Coupled effects are extremely overt for yaw drift forces. In Fig. 9, gap distance plays an important role. When the gap distance is more than 9 m, the coupled drift forces are quite small. On the other hand, change in amplitude of coupled cases within a separation distance of 9m is quite drastic. Additionally, it is easy to find that yaw drift forces of the single body cases in beam waves are nearly zero. However, the coupled drift forces have very large spikes. It again illustrates that beam wave is the most dangerous condition for side-by-side operations.

In the low frequency area where the wave length is large, the diffraction of waves is obvious, thus reducing the wave forces exerted on the vessel. It is seen in all sway and yaw cases, the forces are very small when the non-dimensional frequency is small than 1.0. As the frequency increases, the diffraction of waves is undermined and waves begin to have evident effects on the vessels.

In sum, the degree of discrepancy is drastic between single body cases and multi-body cases near the resonance frequencies for mean drift forces, especially when the two vessels are situated abreast with a small gap distance of 4 m in Figs. 8(h) and 9(h) where the increase of peak values are significant, reaching the highest point at 18.2 and -463.5 respectively at a non-dimensional frequency of 2.33, i.e., 1.10 rad/s. Thus, for vessels in close proximity, the mean drift forces are particularly important. Over many cycles of the first order oscillatory motions, the drift forces may cause substantial changes in the relative positions, possibly leading to collisions. In addition, the separation distance is essential in deciding the coupled drift forces. It can be discerned from the cases of 4m, 6m and 9m that small decrease in gap distances may result in intense increase in drift forces. Therefore, in engineering practice, the operation separation distance should be chosen with caution. It is suggested to expand the gap distance reasonably in order to reduce the coupled drift forces effectively. Since the horizontal mean drift force is one of the most mainly concerned forces to be counteracted in DP system and mooring system, prudent prediction is also helpful in saving the consumed power of DP system and reducing the tension of mooring lines.

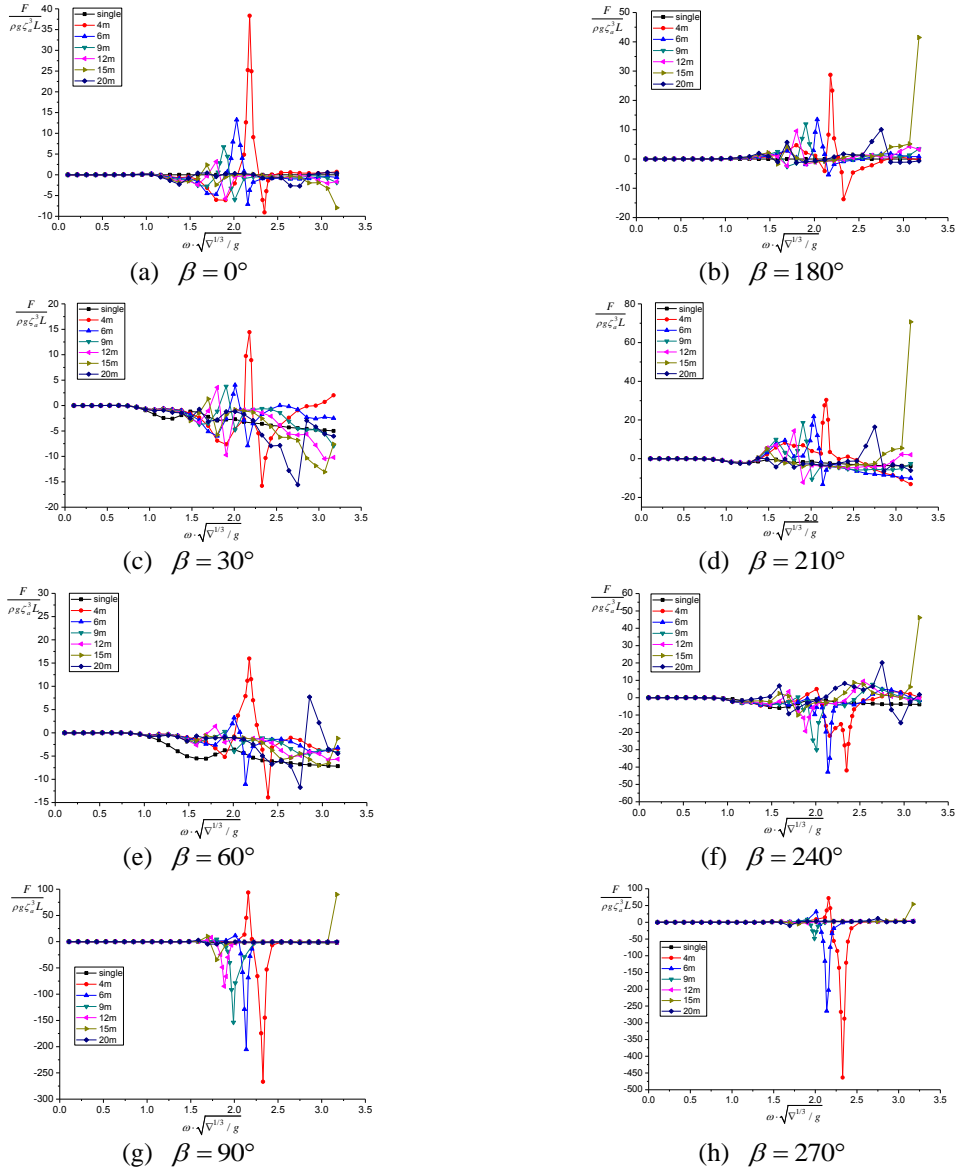


Fig. 9 Yaw mean drift forces of shuttle tanker with different wave directions and spacing distances

5. Conclusions

From the analysis above, the hydrodynamics between two vessels is obviously distinguished from the single body case with shielding and exaggerating effects. With the FPSO and the shuttle tanker getting close, the hydrodynamic interactions between the two vessels are noticeable, especially for sway and yaw directions. Moreover, the sway mean drift forces of multiple body case experience variations in both magnitude and direction. Special attentions should also be paid

to the second peaks of sway RAOs on account of the fact that the motion responses exhibit remarkable rise at resonance frequencies where the results tend to be low for the single body cases.

In conclusion, the gap distance and the wave direction are the predominant determinants compared with other factors. When two vessels are situated side-by-side, either a gap distance of 4m or beam waves contributes more to the hydrodynamic interactions between two vessels than other factors. In consequent, it is extremely adverse when the determinant factors combine to determine the hydrodynamic behaviors of the shuttle tanker. In engineering practice, it is advisable to choose side-by-side operation direction to head and stern waves and the operation distance should be decided with caution to avoid dangerous situation happening.

References

- Chen, X.B. (2007), "Middle-field formulation for the computation of wave-drift loads", *J. Eng. Math*, **59**(1), 61-82.
- Choi, Y.R. and Hong, S.Y. (2002), "An analysis of hydrodynamic interaction of floating multi-body using higher-order boundary element method", *Proceedings of the 12th ISOPE*, Kitakyushu, Japan.
- Dai, Y.S. (1998), *Potential flow theory of ship motions in waves in frequency and time domain (in Chinese)*, Press of the National Defense Industries, Beijing, China.
- Huijsmans, R.H.M., Pinkster, J.A. and de Wilde, J.J. (2001), "Diffraction and radiation of waves around side-by-side moored vessels", *Proceedings of the 11th ISOPE*, Stavanger, Norway.
- Kang, H.Y. and Kim, M.H. (2012), "Hydrodynamic interactions and coupled dynamics between a container ship and multiple mobile harbors", *Ocean Syst. Eng.*, **2**(3), 217-228.
- Kodan, N. (1984), "The motions of adjacent floating structures in oblique waves", *Proceedings of the 3rd Offshore Mechanics and Arctic Engineering*, New Orleans, USA.
- Kristiansen, T. and Faltinsen, O.M. (2010), "A two-dimensional numerical and experimental study of resonant coupled ship and piston-mode motion", *Appl. Ocean Res.*, **32**(2), 158-176.
- Lee, S.J., Kim, M.H., Lee, D.H., Kim, J.W. and Kim, Y.H. (2007), "The effects of LNG-tank sloshing on the global motions of LNG carriers", *J. Ocean Eng.*, **34**(1), 10-20.
- Lu, L., Teng, B., Sun, L. and Chen, B. (2011), "Modeling of multi-bodies in close proximity under water waves- Fluid forces on floating bodies", *J. Ocean Eng.*, **38**(13), 1403-1416.
- Malenica, Š. and Chen, X.B. (1998), *On the irregular frequencies appearing in wave diffraction-radiation solutions*, International Offshore and Polar Engineering, Montreal, Canada.
- Masashi, K. (2005), "Wave drift forces and moments on two ships arranged side by side in waves", *J. Ocean Eng.*, **32**(5-6), 529-555.
- Mirela, Z. (2007), "Sloshing effects accounting for dynamic coupling between vessel and tank liquid motion", *Proceedings of the 26th OMAE*, San Diego, USA.
- Newman, J.N. (1992), "The approximation of free-surface Green functions", *Proceedings of the F. Ursell Retirement Meeting*, Cambridge University Press.
- Noblesse, F. (1982), "The Green function in the theory of radiation and diffraction of regular waves by a body", *J. Eng. Math*, **16**(2), 137-169.
- Ohkusu, M. (1976), "Ship motions in vicinity of a structure", *Proceedings of the 1st International Conference on the Behavior of Off-Shore Structures*, Trondheim, Norway.
- Zhao, W.H., Yang J.M. and Hu Z.Q. (2012), "Hydrodynamic interaction between FLNG Vessel and LNG Carrier in side by side configuration", *J. Hydrodynamics*, **24**(5), 649-657.